PERGAMON

International Journal of Heat and Mass Transfer 45 (2002) 3321–3330

International Journal of HEAT and MASS TRANSFER

www.elsevier.com/locate/ijhmt

A non-uniform temperature non-uniform pressure dynamic model of heat and mass transfer in compact adsorbent beds

L. Marletta [a], G. Maggio [b], A. Freni [b], M. Ingrasciotta [a], G. Restuccia [b,*]

[a] *Dipartimento di Ingegneria Industriale e Meccanica, Università di Catania, Viale Andrea Doria 6, 95125 Catania, Italy*
[b] *CNR – Istituto di Tecnologie Avanzate per l'Energia, "Nicola Giordano", S. Lucia sopra Contesse, 98126 Messina, Italy*

Received 17 November 2001; received in revised form 23 January 2002

Abstract

This paper discusses a new dynamic two-dimensional model for the simulation of innovative consolidated-type adsorbent beds to use in adsorption energy systems. It consists of a cylindrical pipe, conveying the thermal vector fluid, coated with a layer of consolidated zeolite.

The governing equations take into account with detail the transport phenomena and are solved according to advanced numerical methods in the time and space domain.

A parametric analysis is carried out for the evaluation of the overall system performance sensitivity to the most meaningful parameters, such as adsorbent bed thickness, water vapour permeability and heat transfer coefficients. A critical discussion is also made about the most credited adsorbent bed arrangements, i.e., pure powder, consolidated powder and metal bound consolidated powder. It was possible to demonstrate that the adsorbent bed, of consolidated powder type, proposed by the CNR-ITAE Lab, performs better than other bed arrangements available in the literature.

1. Introduction

Heat pumps and air conditioning systems, based on adsorption phenomena of gas on solids, are sound alternatives to vapour-compression systems, for both civil and industrial applications. Indeed they use safe and non-pollutant refrigerants (e.g. water) instead of chlorofluorocarbons (CFCs) and medium to low temperature heat (100–200 °C) as energy source.

However, these systems are affected by a number of critical issues, such as discontinuous operation, low heat transfer between the external source and the porous solid and, finally, the operating pressure, which is fairly lower than the atmospheric value.

An adsorption heat pump performs a closed cycle and requires primary energy in the form of heat. This is usually provided by a stream of hot oil which is not involved in the adsorption/desorption process but activates it by flowing in a pipe bundle immersed in the solid adsorbent (e.g. zeolite).

The adsorbent may be in the form of grain or pellets. With this arrangement the heat transfer is poor because of a number of reasons, such as low convective heat transfer coefficient at the interface oil/metal h_{fm}; low equivalent thermal conductivity λ_{eq} of the granular bed; weak contact between the exchanger surface and the solid grains, which implies low heat transfer coefficients at the interface metal/adsorbent h_{ms}.

The large number of predictive tools available in the literature [1–6] are mostly one-dimensional models and suitable under restricted operating conditions.

To overcome the drawbacks mentioned above and improve the performance of the overall system, several solutions have been proposed. The most promising

* Corresponding author. Tel.: +39-090-624-231/229; fax: +39-090-624-247.

E-mail address: restuccia@itae.me.cnr.it (G. Restuccia).

0017-9310/02/$ - see front matter
PII: S0017-9310(02)00045-5

Nomenclature

a	($= \lambda/\rho c_p$) thermal diffusivity ($m^2\ s^{-1}$)
A	contact area (m^2)
c_p	specific heat ($J\ kg^{-1}\ K^{-1}$)
COP	coefficient of performance
d_{pore}	average pore diameter (m)
D^*	molecular diffusivity ($m^2\ s^{-1}$)
D_v	gaseous effective diffusivity ($m^2\ s^{-1}$)
D_K	Knudsen diffusivity ($m^2\ s^{-1}$)
D_p	adsorbent particle diameter (m)
h	convective heat transfer coefficient ($W\ m^{-2}\ K^{-1}$)
H	specific enthalpy ($J\ kg^{-1}$)
J	mass flow rate ($mol\ m^{-2}\ s^{-1}$)
k_D	porous medium permeability (m^2)
k_E	inertial effect term; Eq. (6) (m)
L	axial length of the adsorber (m)
m	mass (kg)
M	number of axial grid subdivisions
MM	molar mass ($g\ mol^{-1}$)
n	momentum ($kg\ m\ s^{-1}$)
N	number of radial grid subdivisions
p	pressure (Pa)
P	power (W)
q	adsorbed vapour per solid adsorbent solid unit ($kg\ m^{-3}$); thermal source in Eq. (2) (W)
r	mass source in Eq. (1) ($kg\ s^{-1}$); radial co-ordinate (m)
R	universal gas constant ($J\ kg^{-1}\ K^{-1}$)
R_e	adsorber external radius (m)
R_i	adsorber internal radius (m)
s	adsorbent coating thickness (m)
t	time (s)
T	temperature (K)
u_f	fluid velocity ($m\ s^{-1}$)
v	vapour diffusive velocity ($m\ s^{-1}$)
v_0	vapour superficial diffusive velocity ($m\ s^{-1}$)
V	volume (m^3)
w	uptake ($kg\ kg^{-1}$)
z	axial co-ordinate (m)
Z	dimensionless axial co-ordinate

Greek symbols

ΔH	adsorption enthalpy ($J\ kg^{-1}$)
Δp	reference pressure variation (Pa)
Δr	grid radial size (m)
Δt	time step (s)
ΔT	reference temperature variation (K)
Δw	uptake variation ($kg\ kg^{-1}$)
Δz	grid axial size (m)
ε_{ma}	macroporosity
ε_{mi}	microporosity
ϕ	dissipative term
η_T	tortuosity factor
λ	thermal conductivity ($W\ m^{-1}\ K^{-1}$)
μ	dynamic viscosity ($N\ s\ m^{-2}$)
v	velocity ($m\ s^{-1}$)
π	dimensionless pressure
θ	dimensionless temperature
ρ	density ($kg\ m^{-3}$)
σ	collision diameter for Lennard–Jones potential (Å)
τ	dimensionless time
Ω_D	collision integral
Ξ	dimensionless radial co-ordinate
ψ	dimensionless adsorbed vapour

Subscripts

0	initial state
a	adsorbed phase; apparent value
c	cooling
con	condenser
ev	evaporator
eq	equivalent
f	fluid
h	heating
i	i-th phase; grid index in radial direction
inb	inlet oil during heating
inu	inlet oil during cooling
j	grid index in axial direction
m	metal tube
r	radial direction
s	solid adsorbent
v	vapour phase
z	axial direction

approach seems to be the consolidated bed [7]. However, with this arrangement the mass transfer becomes the limiting factor, due to the high thickness of the bed.

In this framework and on the basis of previous experience in the design of consolidated adsorbent beds [8,9], at CNR-ITAE Research Laboratories, has been studied an innovative thin adsorbent coating, based on zeolite (consolidated with an inorganic binder) and bound around a metal tube [10]. This configuration (Fig. 1) allows a slight improvement of the adsorbent thermal conductivity λ_{eq} but a large increase in the metal/adsorbent heat transfer h_{ms}, due to the metal/adsorbent adhesion. Further, the use of a thin coating reduces the path for the vapour diffusion.

The aim of this paper is to propose a mathematical model, able to describe in a proper way the heat and

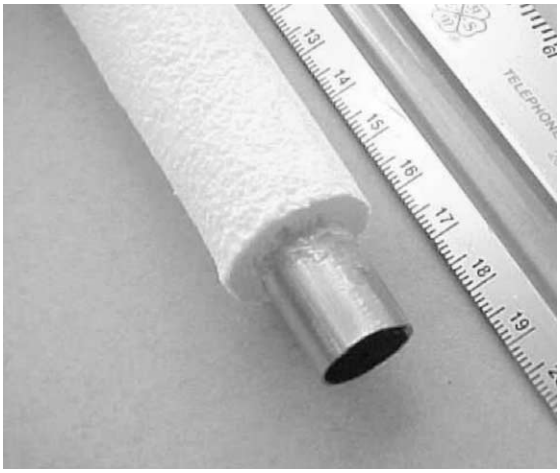

Fig. 1. Representative photo of the consolidated metal-bound zeolite layer (stainless steel tube AISI 304 coated with zeolite 4A 5 mm thick).

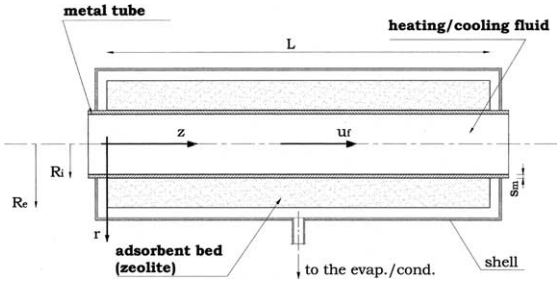

Fig. 2. Scheme of the adsorber basic elements.

- mass balance

$$\frac{\partial m_i}{\partial t} + \vec{\nabla}\vec{n}_i = r_i, \tag{1}$$

- energy balance

$$\frac{\partial}{\partial t}(m_i H_i) + \vec{\nabla}\left(m_i H_i \vec{v}_i\right) = V_i \vec{\nabla}(\lambda_i \vec{\nabla} T) - V_i \vec{\nabla}\left(p_i \vec{v}_i\right) + V_i \mu_i \phi_i + q_i. \tag{2}$$

mass transfer occurring in this new arrangement of the consolidated bed for the zeolite/water pair.

Contrary to other literature models that neglect the resistance to mass diffusion and therefore consider a uniform pressure treatment [1,2], the proposed model concerns the hypothesis of non-uniform temperature and non-uniform pressure within the adsorbent bed.

The set of heat and mass transfer equation is solved according to advanced and suitable numerical methods, such as to prevent convergence and stability problems.

The meaningful results obtained through computer simulations are discussed. First a parametric analysis of a base-case system for the most relevant design parameters is performed, and finally a comparison of the proposed metal bound consolidated powder with other adsorbent bed arrangements presented in the literature is realised.

2. Model assumptions

Fig. 2 shows a scheme of the adsorbent bed. It is possible to recognise the three main elements, relevant for the mathematical model: the thermal vector fluid, the metal tube and adsorbent material. The latter includes a porous solid and the water vapour both in gaseous and adsorbate phase. The size of the zeolite coating is defined by $R_e - R_i$ and L.

The phenomena to describe are related to a heat transfer, which involves all the elements mentioned above, and a mass transfer which concerns only the gaseous phase through the pores of the adsorbent. Thus, with reference to the ith species flowing with velocity $\vec{v}_i$, the following relationships [11,12] hold:

The following assumptions are made:

(a) All the adsorbent particles have the same properties (including shape and size); they are uniformly distributed throughout the adsorbent, and in local thermal equilibrium with the adsorbate and the surrounding vapour phase ($T_s = T_v$).
(b) The oil and the metal thermal gradients in radial direction are neglected; the corresponding equations become one-dimensional.
(c) The gaseous phase behaves as an ideal gas.
(d) The properties of the metal and the gaseous phase are assumed constant.
(e) The properties of the thermal vector fluid, as well as those of the adsorbent, are considered temperature dependent.
(f) All the thermal losses are negligible.

This model treats some parameters in a more rigorous form than usual. In particular, experimentally measured values are adopted for the thermal conductivity of the zeolite [9] and the contact resistance at the tube–zeolite interface [10].

The adsorption enthalpy is not considered constant, as often occurs in literature, but dependent on the uptake [13].

The equivalent specific heat (c_{peq}) of the adsorbent is considered to be a function of the uptake and temperature. It was determined by experimental measurements [14]. Such an approach avoids the uncertainty related to the usual hypothesis of attributing to the adsorbate the specific heat of liquid or water vapour.

Eq. (1) must be coupled with a further equation that relates the mass flow to its driving force.

It should be noted that generally the driving force for the mass transfer may be a pressure and/or a concentration gradient [11,12]. The proper physical relationships, respectively, are the Darcy's ($\vec{v} = -(k_D/\mu_v)\vec{\nabla}p$) and Fick's ($\vec{J} = -D_v\vec{\nabla}c$) laws, being k_D the permeability and D_v the diffusivity. To treat the two phenomena together, it is convenient to introduce an apparent permeability [15,16] defined as follows:

$$k_{D_{eq}} = k_D + k_a = k_D + \frac{D_v\mu_v}{p}. \tag{3}$$

Further, Ergun's equation [11] was used, because it is more general than Darcy's law and most suitable for porous solids.

$$\vec{v}_0 + \frac{\rho_v}{\mu_v}k_E\vec{v}_0\left|\vec{v}_0\right| = -\frac{k_{D_{eq}}}{\mu_v}\vec{\nabla}p. \tag{4}$$

In these equations k_D is the real permeability and k_E is a parameter taking into account the inertial effects. They are defined as follows [11]:

$$k_D = \frac{\varepsilon_{ma}^3 D_p^2}{150(1-\varepsilon_{ma})^2} \tag{5}$$

and

$$k_E = \frac{1.75D_p}{150(1-\varepsilon_{ma})}. \tag{6}$$

The diffusion coefficient D_v, appearing in Eq. (3), depends on the diffusion mechanism. By considering a mass transfer controlled by the macropore diffusion, for a single-component gas the effective diffusivity is defined as [17–20]

$$D_v = \left(\frac{1}{D^*} + \frac{1}{D_K}\right)^{-1}\frac{\varepsilon_{ma}}{\eta_T} \tag{7}$$

with

$$D^* = 0.02628\frac{\sqrt{T^3/MM_v}}{p\sigma^2\Omega_D} \qquad \text{self-diffusion [20]},$$

$$D_K = 48.5d_{pore}\sqrt{\frac{T}{MM_v}} \qquad \text{Knudsen diffusion}.$$

Finally, the adsorbent/adsorbate water equilibrium is represented by the following equation:

$$\ln p = A(w) + \frac{B(w)}{T}, \tag{8}$$

where $A(w)$ and $B(w)$ are cubic polynomials with coefficients obtained experimentally and available in literature [13].

3. Model equations

Based on the previous assumptions, Eqs. (1) and (2) become

(a) *Energy balance for the thermal vector fluid*

$$\frac{\partial T_f}{\partial t} + u_f\frac{\partial T_f}{\partial z} - a_f\frac{\partial^2 T_f}{\partial z^2} + \frac{h_{fm}A_{fm}}{\rho_f c_{pf}V_f}(T_f - T_m) = 0. \tag{9}$$

(b) *Energy balance for the metal tube*

$$\frac{\partial T_m}{\partial t} - a_m\frac{\partial^2 T_m}{\partial z^2} + \frac{h_{fm}A_{fm}}{\rho_m c_{pm}V_m}(T_m - T_f) + \frac{h_{ms}A_{ms}}{\rho_m c_{pm}V_m} \times (T_m - T_{s|m}) = 0. \tag{10}$$

(c) *Mass balance for the adsorbent*

$$\left\{[\varepsilon_{ma} + (1-\varepsilon_{ma})\varepsilon_{mi}]\frac{1}{RT_s} + (1-\varepsilon_{ma})(1-\varepsilon_{mi})\left.\frac{\partial q_a}{\partial p}\right|_{T_s}\right\}\frac{\partial p}{\partial t} - \left\{[\varepsilon_{ma} + (1-\varepsilon_{ma})\varepsilon_{mi}]\frac{p}{RT_s^2} - (1-\varepsilon_{ma})(1-\varepsilon_{mi})\left.\frac{\partial q_a}{\partial T_s}\right|_{p}\right\} \times \frac{\partial T_s}{\partial t} + \frac{1}{r}\frac{\partial}{\partial r}\left(r\frac{v_{0r}p}{RT_s}\right) + \frac{\partial}{\partial z}\left(\frac{v_{0z}p}{RT_s}\right) = 0. \tag{11}$$

(d) *Energy balance for the adsorbent*

$$\left\{[\varepsilon_{ma} + (1-\varepsilon_{ma})\varepsilon_{mi}]\frac{c_{pv}}{R} - (1-\varepsilon_{ma})(1-\varepsilon_{mi}) \times \left[|\Delta H| - \left(c_{peq} + (\rho_s + q_a)\left.\frac{\partial c_{peq}}{\partial q_a}\right|_{T_s}\right)T_s\right]\left.\frac{\partial q_a}{\partial p}\right|_{T_s}\right\}\frac{\partial p}{\partial t} + (1-\varepsilon_{ma})(1-\varepsilon_{mi})\left\{(\rho_s + q_a)\left(c_{peq} + T_s\left.\frac{\partial c_{peq}}{\partial T_s}\right|_{q_a}\right) - \left[|\Delta H| - \left(c_{peq} + (\rho_s + q_a)\left.\frac{\partial c_{peq}}{\partial q_a}\right|_{T_s}\right)T_s\right]\left.\frac{\partial q_a}{\partial T_s}\right|_{p}\right\}\frac{\partial T_s}{\partial t} + \frac{1}{r}\frac{\partial}{\partial r}\left[r\left(\frac{c_{pv}}{R} + 1\right)pv_{0r}\right] + \frac{\partial}{\partial z}\left[\left(\frac{c_{pv}}{R} + 1\right)pv_{0z}\right] = \lambda_{eq}\left[\frac{1}{r}\frac{\partial}{\partial r}\left(r\frac{\partial T_s}{\partial r}\right) + \frac{\partial^2 T_s}{\partial z^2}\right], \tag{12}$$

where $T_{s|m}$ is the adsorbent temperature at the solid/metal interface.

By solving the set of differential Eqs. (9)–(12) in time and space, the following unknowns are found: T_f, thermal vector fluid temperature; T_m, metal tube temperature; T_s, adsorbent temperature; p, adsorbent pressure.

Accordingly it is possible to calculate the uptake distribution, the amounts of heat exchanged and, consequently, the performance of a given adsorption system.

To complete the mathematical formulation of the problem, the initial and boundary conditions are reported below.

For $t = 0 \quad T_f(z) = T_m(z) = T_s(r,z) = T_0$

and

$$p = p_0, \tag{13}$$

$$T_{\mathrm{f}}|_{z=0} = \begin{cases} T_{\mathrm{inb}} & \text{for the heating phase,} \\ T_{\mathrm{inu}} & \text{for the cooling phase,} \end{cases} \tag{14}$$

$$\left.\frac{\partial T_{\mathrm{f}}}{\partial z}\right|_{z=L} = 0, \tag{15}$$

where T_{inb} is the temperature of the thermal source, and T_{inu} that of the user.

$$\left.\frac{\partial T_{\mathrm{m}}}{\partial z}\right|_{z=0} = \left.\frac{\partial T_{\mathrm{m}}}{\partial z}\right|_{z=L} = 0, \tag{16}$$

$$\left.\frac{\partial T_{\mathrm{s}}}{\partial z}\right|_{z=0} = \left.\frac{\partial T_{\mathrm{s}}}{\partial z}\right|_{z=L} = \left.\frac{\partial T_{\mathrm{s}}}{\partial r}\right|_{r=R_{\mathrm{e}}} = 0, \tag{17}$$

$$-\lambda_{\mathrm{eq}} \left.\frac{\partial T_{\mathrm{s}}}{\partial r}\right|_{r=R_{\mathrm{i}}} = h_{\mathrm{ms}}(T_{\mathrm{m}} - T_{\mathrm{s}}), \tag{18}$$

$$p|_{z=0} = p|_{z=L} = p|_{r=R_{\mathrm{e}}} = p_{\mathrm{ev/con}}$$

for bed connected to the evaporator/condenser, (19)

$$\left.\frac{\partial p}{\partial z}\right|_{z=0} = \left.\frac{\partial p}{\partial z}\right|_{z=L} = \left.\frac{\partial p}{\partial r}\right|_{r=R_{\mathrm{e}}} = 0$$

for closed connections to the evaporator/condenser, (20)

where $p_{\mathrm{ev/con}}$ is the pressure of the evaporator or the condenser, which can be calculated as a function of the corresponding temperatures, based on the water vapour pressure.

To simplify the solution of the problem, Eqs. (9)–(12) can be arranged in a dimensionless form. Once the dimensionless variables and parameters specified in the Appendix A have been introduced, the following equations are obtained:

$$\frac{\partial \theta_{\mathrm{f}}}{\partial \tau} + \frac{\partial \theta_{\mathrm{f}}}{\partial Z} - \frac{1}{Pe_{\mathrm{f}}} \frac{\partial^2 \theta_{\mathrm{f}}}{\partial Z^2} + \mathrm{NTU_f}(\theta_{\mathrm{f}} - \theta_{\mathrm{m}}) = 0, \tag{21}$$

$$\frac{\partial \theta_{\mathrm{m}}}{\partial \tau} - \frac{1}{Pe_{\mathrm{m}}} \frac{\partial^2 \theta_{\mathrm{m}}}{\partial Z^2} + \varphi \mathrm{NTU_f}(\theta_{\mathrm{m}} - \theta_{\mathrm{f}}) + \mathrm{NTU_m}\left(\theta_{\mathrm{m}} - \theta_{\mathrm{s|m}}\right) = 0, \tag{22}$$

$$\Lambda_1 \frac{\partial \pi}{\partial \tau} + \Lambda_2 \frac{\partial \theta_{\mathrm{s}}}{\partial \tau} = \frac{\Delta_{1\mathrm{r}}}{\Xi} \frac{\partial \pi}{\partial \Xi} + \frac{\partial}{\partial \Xi}\left(\Delta_{1\mathrm{r}} \frac{\partial \pi}{\partial \Xi}\right) + \frac{\partial}{\partial Z}\left(\Delta_{1z} \frac{\partial \pi}{\partial Z}\right), \tag{23}$$

$$\Lambda_3 \frac{\partial \pi}{\partial \tau} + \Lambda_4 \frac{\partial \theta_{\mathrm{s}}}{\partial \tau} = \frac{\Delta_{2\mathrm{r}}}{\Xi} \frac{\partial \pi}{\partial \Xi} + \frac{1}{\Xi Pe_{\mathrm{r}}} \frac{\partial \theta_{\mathrm{s}}}{\partial \Xi} + \frac{\partial}{\partial \Xi}\left(\Delta_{2\mathrm{r}} \frac{\partial \pi}{\partial \Xi}\right) + \frac{\partial}{\partial Z}\left(\Delta_{2z} \frac{\partial \pi}{\partial Z}\right) + \frac{\partial}{\partial \Xi}\left(\frac{1}{Pe_{\mathrm{r}}} \frac{\partial \theta_{\mathrm{s}}}{\partial \Xi}\right) + \frac{\partial}{\partial Z}\left(\frac{1}{Pe_z} \frac{\partial \theta_{\mathrm{s}}}{\partial Z}\right). \tag{24}$$

4. Solution of the mathematical model

The set of second-order partial differential equations (PDEs) mentioned above can be solved by numerical methods [21–24].

The adsorber is described with a grid of $M \times N$ elementary areas. These have size Δz ($\Delta z = L/M$) in axial direction and Δr ($\Delta r = (R_{\mathrm{e}} - R_{\mathrm{i}})/N$) in radial direction and are small enough to neglect the variations of the temperature and pressure in each one.

The dimensionless equations were discretised using the following schemes: forward difference scheme (FDS) for time derivatives and boundary conditions, quickest upstream difference scheme (QUDS, proposed by Leonard [23], which proved to be accurate and stable) for spatial first-order derivatives, central difference scheme (CDS) for spatial second-order derivatives.

The non-linearity of the Eqs. (23) and (24), due to the time dependence of the coefficients $\Lambda_1, \Lambda_2, \Lambda_3, \Lambda_4$, $\Delta_{1\mathrm{r}}, \Delta_{1z}, \Delta_{2\mathrm{r}}$ and Δ_{2z}, has been overcome by iterative techniques.

With regard to the solution, the alternating direction implicit (ADI) method [21] was used. Since this is an implicit method, the function to be calculated at any given time depends on the physical state of the surrounding meshes at the same time, and on that of the previous time step. Thus, at each time, the solution of a system of equations allows to determine the values of the unknown function in the whole domain.

Another typical feature of the method is the splitting of the time step in two half steps, in each of which the equations are considered not stationary and one-dimensional (two independent variables).

It should be noted that the matrices of the linear algebraic systems of equations corresponding to each time step have many zero elements (sparse matrices). In this condition, it is suitable to use the biconjugate gradient method [24], which allows accurate and fast results.

In conclusion, starting from the known thermopressure conditions of the initial time, the simulation model calculates, in time and space, the pressure distribution within the adsorbent and the temperature profile in the oil, in the metal tube and the adsorbent itself. Then, determines the uptake distribution, the average values of the above variables and the heat transfer rate. The overall system performance can be finally assessed by means of a procedure, based on previous formulations [13,25,26] here adapted to a dynamic model.

5. Discussion on parameters affecting the numerical resolution

The input data related to numerical aspects are collected on the topside of Table 1, whereas other

Table 1
Model input data

Parameter	Symbol	Value	Ref.
Input data relevant to numerical aspects			
Reference temperature	T_R	20 °C	–
Reference pressure	p_R	1000 Pa	–
Reference temperature variation	ΔT	1 °C	–
Reference pressure variation	Δp	1 Pa	–
Time step	Δt	0.01 s	–
Number of axial subdivisions	M	10	–
Number of radial subdivisions	N	15	–
Thermophysical properties and structural characteristics			
Zeolite bulk density	ρ_s	960 kg m^{-3}	Experim.
Equivalent (zeolite + water) thermal conductivity	λ_{eq}	0.3 W m^{-1} K^{-1}	Experim.
Metal/zeolite heat transfer coefficient	h_{ms}	180 W $m^{-2}K^{-1}$	[29]
Average macropore diameter	d_{pore}	0.7 μm	Experim.
Macroporosity	ε_{ma}	0.315	Experim.
Microporosity	ε_{mi}	0.42	[30]
Particle equivalent diameter	D_p	200 μm	Assumed
Operative conditions and adsorber geometry			
Initial temperature	T_0	45 °C	–
Initial adsorber pressure	p_0	879 Pa	–
Cycle maximum temperature	T_{max}	200 °C	–
Cycle minimum temperature	T_{min}	45 °C	–
Evaporator temperature	T_{ev}	5 °C	–
Condenser temperature	T_{con}	45 °C	–
Inlet oil temperature during heating	T_{inb}	210 °C	–
Inlet oil temperature during cooling	T_{inu}	35 °C	–
Metal tube internal radius	R_f	8 mm	–
Metal tube external radius	R_i	9 mm	–
Adsorber external radius	R_e	14 mm	–
Adsorber axial length	L	500 mm	–
Oil velocity	u_f	1 m s^{-1}	–

parameters, typical for such systems, are reported on the bottom of the table.

The influence of the calculation time step and of the grid size on the model results has been widely analysed by numerous simulations. Inspection of these results demonstrates that the numerical problems are limited to a few extreme cases: when a too large value of the time step is considered (in particular, $\Delta t = 1$ s) or when the number of grid subdivisions is not adequate. Moreover, by examining the spatial local distributions, it has been realised that the effect due to the boundary conditions remain limited to the borders of the adsorber.

The periodic stability of the parameters that describe the thermodynamic cycle was also ascertained, by calculating and plotting their profiles for several cycles.

Based on these considerations, a time step $\Delta t = 0.01$ s and a grid $M \times N = 10 \times 15$ were chosen to warrant the consistence of the results.

6. Results of the base-case simulation

This section discusses the first results, obtained for a specific assembly referred to as base-case. The most relevant input data are collected in Table 1 together with the data used as numerical parameters whose influence on the solution have been already discussed. The zeolite 4A/water was adopted as the adsorbent/adsorbate pair.

The typical profile of temperature, pressure and uptake, as a function of time, reported in Figs. 3 and 4, put in evidence that:

- the cycle duration is 926 s;
- the effect of the heat transfer resistances ($1/h_{fm}$, $1/h_{ms}$ and s/λ_{eq}) is evident from the behaviour of the average temperatures for the three components;
- due to the mass transfer resistance, the average pressure during the adsorption phase is not constant. This is well established from Fig. 5, where a comparison is made of the actual path (dotted line) with the

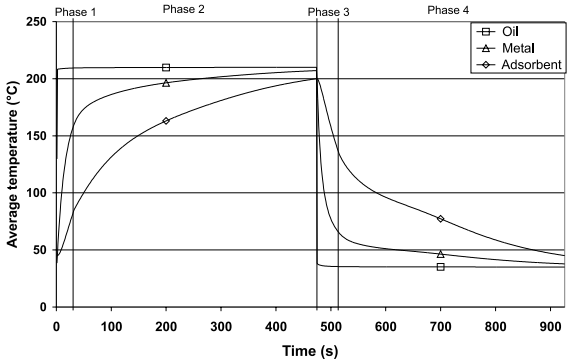

Fig. 3. Average temperatures vs. time in one cycle period.

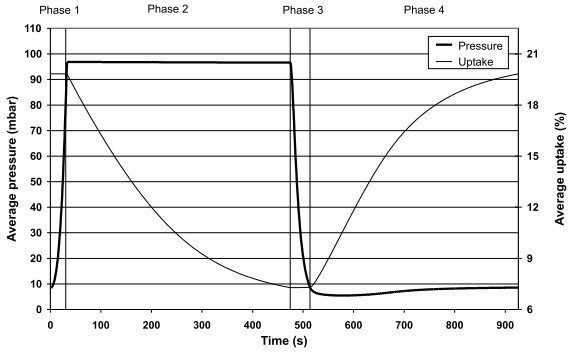

Fig. 4. Average pressures and uptakes vs. time in one cycle period.

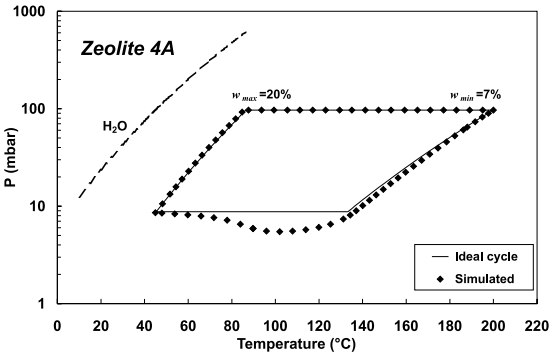

Fig. 5. Comparison of the ideal and simulated cycles.

ideal one (solid line). Actually, although is enhanced in terms of visibility, by the adopted log scale, the difference in pressure between the two paths in the adsorption phase, is small (less than 3 mbar). During the other phases, the behaviour of the average pressure is in agreement with the expectations.

Fig. 6 shows the heat transfer rate as a function of time for the four phases of the thermal cycle. The results need

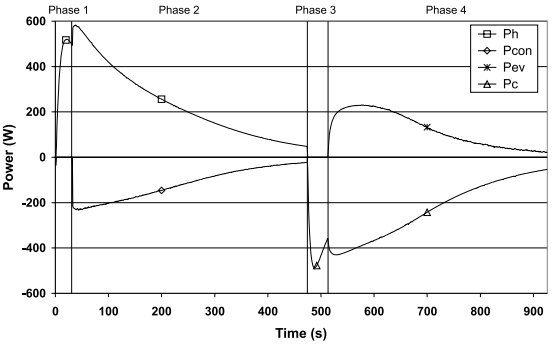

Fig. 6. Thermal power vs. time for the base-case in one cycle period.

no special remark unless for the P_h curve which, after a strong initial increase, begins reducing at the end of the isosteric heating, since the difference of temperature adsorbent/oil diminishes.

The calculated power is qualitatively in agreement with those determined by other models of global dynamic simulation [27].

The coefficients of performance (COP) calculated by the model are: $COP_c = 0.43$ for cooling mode, and $COP_h = 1.37$ for heating mode (the adopted operative conditions are $T_{min} = T_{con} = 45$ °C, $T_{ev} = 5$ °C, $T_{max} = 200$ °C for cooling and $T_{min} = T_{con} = 55$ °C, $T_{ev} = 7$ °C, $T_{max} = 200$ °C for heating). These values are in a good agreement with the calculations of a previous model [13] based on the ideal cycle and other models available in the literature [25,27,28].

7. Sensitivity analysis

The sensitivity analysis was carried out with reference to the parameters listed in Table 2; all other data are those pertaining to the base-case. In the following sections the most relevant results are discussed.

Table 2
Sensitivity analysis simulations

Case	R_s (mm)	D_p (μm)	Adsorbent configuration
Base-case	14	200	Tile on metal[a]
Case (1)	12	b.c.	b.c.
Case (2)	16	b.c.	b.c.
Case (3)	b.c.	100	b.c.
Case (4)	b.c.	500	b.c.
Case (5)	b.c.	b.c.	Pure powder[a]
Case (6)	b.c.	b.c.	Metal-bound tile[a]

Symbol b.c. stands for base-case values.

[a] See Table 3 for the values of the corresponding thermal coefficients.

The influence of the zeolite thickness on the thermal cycle was investigated for the following cases: 3, 5 (base-case) and 7 mm. The results show that negligible deviations from the ideal cycle shape occur only during the adsorption phase; further, the thicker is the adsorbent layer, the slightly larger is the deviation. This behaviour may easily be explained by observing that during adsorption the mass transfer rate is the dominant mechanism and the mass resistance is relevant.

The bed thickness affects also the cycle duration. Data, obtained from the simulations, allow to state that when the adsorbent thickness increases, the time necessary for the completion of each phase also increases and so the cycle duration, namely: 460 s for the layer 3 mm thick; 926 s for 5 mm thick and 1547 s for 7 mm thick.

The consequences of the mass transfer resistance in the adsorbent were sought by considering three different values of permeability (k_D), corresponding to different zeolite powder grain size D_p (i.e., case 3, 4 and base-case in Table 2). The results, presented in Fig. 7 show that permeability mostly affects the adsorption phase.

Finally, the influence of λ_{eq} and h_{ms}, on the system performance was evaluated by considering three different adsorbent bed configurations, i.e., (1) pure powder; (2) powder consolidated by a binder (base-case); (3) powder consolidated by a binder and adhered on metal. The first (traditional adsorbent) configuration, is characterised by heat transfer coefficients as low as $\lambda_{eq} = 0.2$ W m^{-1} K^{-1} and $h_{ms} = 45$ W m^{-2} K^{-1}.

Consolidated adsorbents allow a better thermal contact, then $h_{ms} = 180$ W m^{-2} K^{-1}; besides, a proper binder and a fairly high density allow a slight increase in the thermal conductivity ($\lambda_{eq} = 0.3$ W m^{-1} K^{-1}).

The third configuration is the CNR-ITAE Lab type consolidated bed, for which the adsorbent material is firmly bound on the metal by means of a binder; in this conditions metal/adsorbent heat transfer coefficient attains a value as high as $h_{ms} = 1000$ W m^{-2} K^{-1} [10].

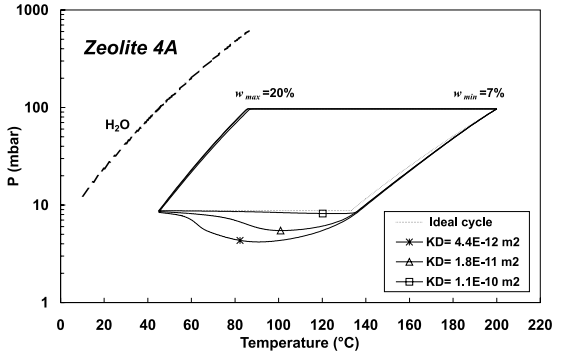

Fig. 7. Influence of the vapour permeability on cycle path.

Table 3
Typical values of thermal coefficients for different adsorbent configurations [7,30,31] and corresponding calculated average specific cooling power

Adsorbent configuration	λ_{eq} (W m^{-1} K^{-1})	h_{ms} (W m^{-2} K^{-1})	Power (W kg^{-1})
Pure powder	0.2	45	141
Tile on metal	0.3	180	312
Metal-bound tile	0.3	1000	432

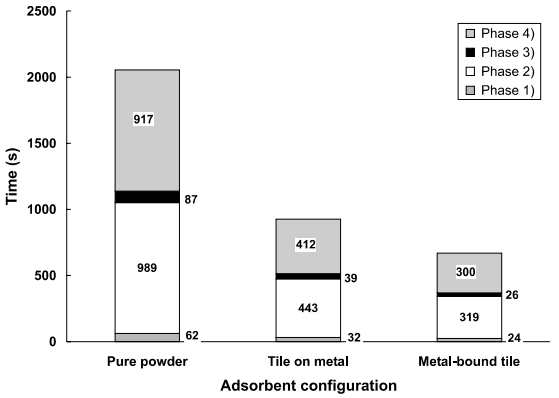

Fig. 8. Duration of each cycle phase for three adsorbent bed arrangements.

Table 3 collects the adopted values of the thermal parameters corresponding to the three examined configurations.

The results, for the three arrangements, are shown in Fig. 8 and are self-evident.

The shortest cycle duration is owing to the CNR-ITAE assembly, and is certainly attributable to the excellent heat transfer conditions provided by the metal bound consolidated powder arrangement.

The specific power (per adsorbent mass unit) results in 432 W kg^{-1} for the CNR-ITAE bed type against 141 W kg^{-1} for the pure powder (Table 3). This further confirms the better performance of the proposed design with respect to the other traditional configurations.

8. Conclusions

This paper deals with adsorption systems. These are promising alternatives to conventional systems for heating and cooling purposes. Indeed they guarantee quite and reliable operation and may provide substantial help in reducing pollutant emissions.

Still they are affected by some technical drawbacks that actually reduce their overall performance. Among these, the contact resistance at the tube/adsorbent interface and the heat and mass transfer resistance within the adsorbent bed deserve a special mention.

To overcome these problems the CNR-ITAE Research Lab has recently proposed an innovative adsorbent bed obtained by a thin adsorbent coating, based on zeolite (consolidated with an inorganic binder) bound around a metal tube.

In order to predict the thermal performance of an adsorption machine equipped with such a device, and compare that to other bed arrangements available in the literature, a new mathematical model has been developed.

The model is based on the heat and mass transfer balance equations, stated in two-dimensional and solved in time and space. The reference case was a typical assembly including the zeolite layer, the metal tube and the working fluid.

The model allows an accurate description of heat and mass transfer problems for consolidated-type adsorbents. The consistency of the method has been successfully demonstrated by numerous simulations that have shown the excellent stability and convergence of the model, when varying the spatial grid size and the time step.

A comparison was made with others, more traditional bed designs, such as the pure powder and consolidated powder type. The comparison was made in terms of the thermal cycle shape, cycle duration and specific power released to the user.

It was possible to demonstrate that the proposed consolidated bed performs better than the competing arrangements with respect to all the above-mentioned parameters. Indeed the CNR-ITAE bed type allows a thermal cycle shorter in duration, and more efficient in terms of specific power than other bed configurations proposed in the literature.

Acknowledgements

The work presented here was supported by the CNR Progetto Finalizzato Materiali Speciali per Tecnologie Avanzate II.

Appendix A

To obtain the dimensionless form of the heat and mass balance equations of the adsorber, the following dimensionless variables were introduced:

$$\tau=\frac{u_f t}{L},\quad \Xi=\frac{r}{R_e},\quad Z=\frac{z}{L},\quad \pi=\frac{p-p_R}{\Delta p},$$

$$\theta_s=\frac{T_s-T_R}{\Delta T},\quad \theta_m=\frac{T_m-T_R}{\Delta T},\quad \theta_f=\frac{T_f-T_R}{\Delta T},$$

$$\psi=\frac{q_a R\Delta T}{\Delta p}$$

and the dimensionless parameters:

$$\sigma_r=\frac{R_e}{L},\quad \theta_{inb}=\frac{T_{inb}-T_R}{\Delta T},\quad \theta_{inu}=\frac{T_{inu}-T_R}{\Delta T},$$

$$\pi_R=\frac{p_R}{\Delta p},\quad \theta_R=\frac{T_R}{\Delta T},\quad \Sigma=\frac{k_{D_{eq}}\Delta p}{\mu_v L},\quad Re=\frac{\rho_v \Sigma L}{\mu_v},$$

$$Fs=\frac{k_E}{L},\quad \psi_s=\frac{\rho_s R\Delta T}{\Delta p},\quad \psi_{sa}=\psi_s+\psi,$$

$$Pe_z=\frac{u_f L c_{pv}\Delta p}{\lambda_{eq} R\Delta T},\quad Pe_r=\frac{\sigma_r^2 u_f L c_{pv}\Delta p}{\lambda_{eq} R\Delta T},\quad Pe_f=\frac{u_f L}{a_f},$$

$$Pe_m=\frac{u_f L}{a_m},\quad \varphi=\frac{\rho_f c_{pf} V_f}{\rho_m c_{pm} V_m},$$

$$NTU_f=\frac{L h_{fm} A_{fm}}{u_f \rho_f c_{pf} V_f},\quad NTU_m=\frac{L h_{ms} A_{ms}}{u_f \rho_m c_{pm} V_m},$$

where the Reynolds (Re), Forchheimer (Fs) and Peclet (Pe) numbers can be easily recognised; while NTU_f and NTU_m are the "numbers of transfer unit" for fluid/metal and metal/adsorbent heat transfer.

Lastly, the non-constant dimensionless parameters appearing in the Eqs. (23) and (24) are defined by:

$$\Lambda_1=\frac{\varepsilon_{ma}+(1-\varepsilon_{ma})\varepsilon_{mi}}{\theta_s+\theta_R}+(1-\varepsilon_{ma})(1-\varepsilon_{mi})\left.\frac{\partial\psi}{\partial\pi}\right|_{\theta_s},$$

$$\Lambda_2=-[\varepsilon_{ma}+(1-\varepsilon_{ma})\varepsilon_{mi}]\frac{\pi+\pi_R}{(\theta_s+\theta_R)^2}+(1-\varepsilon_{ma})(1-\varepsilon_{mi})\left.\frac{\partial\psi}{\partial\theta_s}\right|_{\pi},$$

$$\Lambda_3=\varepsilon_{ma}+(1-\varepsilon_{ma})\varepsilon_{mi}-(1-\varepsilon_{ma})(1-\varepsilon_{mi})\times\left\{\frac{|\Delta H|}{c_{pv}\Delta T}-\left[c_{peq}+\psi_{sa}\left.\frac{\partial c_{peq}}{\partial\psi}\right|_{\theta_s}\right]\frac{(\theta_s+\theta_R)}{c_{pv}}\right\}\left.\frac{\partial\psi}{\partial\pi}\right|_{\theta_s},$$

$$\Lambda_4=(1-\varepsilon_{ma})(1-\varepsilon_{mi})\left\{\frac{\psi_{sa}}{c_{pv}}\left[c_{peq}+\left.\frac{\partial c_{peq}}{\partial\theta_s}\right|_{\psi}(\theta_s+\theta_R)\right]-\left\{\frac{|\Delta H|}{c_{pv}\Delta T}-\left[c_{peq}+\psi_{sa}\left.\frac{\partial c_{peq}}{\partial\psi}\right|_{\theta_s}\right]\frac{(\theta_s+\theta_R)}{c_{pv}}\right\}\left.\frac{\partial\psi}{\partial\theta_s}\right|_{\pi}\right\},$$

$$\Delta_{1r}=\frac{K_r\Sigma(\pi+\pi_R)}{\sigma_r^2 u_f(\theta_s+\theta_R)},\quad \Delta_{1z}=\frac{K_z\Sigma(\pi+\pi_R)}{u_f(\theta_s+\theta_R)},$$

$$\Delta_{2r}=\left(\frac{R}{c_{pv}}+1\right)\frac{K_r\Sigma(\pi+\pi_R)}{\sigma_r^2 u_f},$$

$$\Delta_{2z}=\left(\frac{R}{c_{pv}}+1\right)\frac{K_z\Sigma(\pi+\pi_R)}{u_f},$$

$$K_r=\frac{2}{1+\sqrt{1+4\frac{ReFs}{\sigma_r}|\partial\pi/\partial\Xi|}},$$

$$K_z=\frac{2}{1+\sqrt{1+4ReFs|\partial\pi/\partial Z|}},$$

where the last two terms take into account the explicit formulation of the diffusive superficial velocities of the vapour deducible from Eq. (3):

$$v_{0r} = -\frac{2k_{D_{eq}}\mu_v^{-1}\partial p/\partial r}{1+\sqrt{1+4\rho_v k_{D_{eq}} k_E \mu_v^{-2}|\partial p/\partial r|}},$$

$$v_{0z} = -\frac{2k_{D_{eq}}\mu_v^{-1}\partial p/\partial z}{1+\sqrt{1+4\rho_v k_{D_{eq}} k_E \mu_v^{-2}|\partial p/\partial z|}}.$$

References

[1] J.J. Guilleminot, F. Meunier, J. Pakleza, Heat and mass transfer in a non-isothermal fixed bed solid adsorbent reactor: a uniform pressure non-uniform temperature case, Int. J. Heat Mass Transfer 30 (1987) 1595–1606.

[2] L.M. Sun, Y. Feng, M. Pons, Numerical investigation of adsorptive heat pump systems with thermal wave heat regeneration under uniform-pressure conditions, Int. J. Heat Mass Transfer 40 (1997) 281–293.

[3] M. Harkonen, A. Aittomaki, Analytical model for the thermal wave adsorption of heat pump cycle, Heat Recovery Syst. CHP 12 (1992) 73–80.

[4] M. Tatlier, B. Tantekin-Ersolmaz, A. Erdem-Senatalar, A novel approach to enhance heat and mass transfer in adsorption heat pumps using the zeolite-water pair, Microporous Mesoporous Mater. 27 (1999) 1–10.

[5] L.Z. Zhang, L. Wang, Effect of coupled heat and mass transfer in adsorbent on the performance of a waste heat adsorption cooling unit, Appl. Thermal Eng. 19 (1999) 195–215.

[6] A. Hajii, W.M. Worek, Simulation of a regenerative, closed-cycle adsorption cooling/heating system, Energy 16 (1991) 643–654.

[7] J.J. Guilleminot, J.B. Chaflen, A. Choisie, Heat and mass transfer characteristics of composites for adsorption heat pumps, in: Proceedings of the International Absorption Heat Pump Conference, New Orleans, Louisiana, AES-vol. 31, 1994, pp. 401–406.

[8] G. Restuccia, A. Freni, G. Cacciola, Adsorption beds of zeolite on aluminium sheets, in: Proceedings of the International Sorption Heat Pump Conference, Munich, Germany, 1999, pp. 343–347.

[9] L. Pino, Yu. Aristov, G. Cacciola, G. Restuccia, Composite materials based on zeolite 4A for adsorption heat pumps, Adsorption 3 (1996) 33–40.

[10] A. Freni, A. Vita, G. Restuccia, in: 7th European Conference on Advanced Materials and Processes (EUROMAT 2001), CD-Conference Proceedings, ISBN 8885298397, Rimini, Italy, 2001.

[11] R.B. Bird, W.E. Stewart, E.N. Lightfoot, Transport Phenomena, John Wiley and Sons, New York, 1960.

[12] H.D. Baehr, K. Stephan, Heat and Mass Transfer, Springer, Berlin, 1998.

[13] G. Cacciola, G. Restuccia, Reversible adsorption heat pump: a thermodynamic model, Int. J. Refrig. 18 (1995) 100–106.

[14] G. Cacciola, G. Maggio, G. Restuccia, Misura della capacità termica di adsorbenti e calcolo delle prestazioni di pompe di calore ad adsorbimento, La Termotecnica 52 (3) (1998) 67–72.

[15] S.M. Taqvi, A. Vishnoi, M.D. Levan, Effect of macropore convection on mass transfer in a bidisperse adsorbent particle, Adsorption 3 (1997) 127–136.

[16] A. Serbezov, S.V. Sotirchos, Mathematical modeling of multicomponent nonisothermal adsorption in sorbent particles under pressure swing condition, Adsorption 4 (1998) 93–111.

[17] J. Karger, D.M. Ruthven, Diffusion in zeolites and other microporous solids, John Wiley and Sons, London, 1992.

[18] D.M. Ruthven, Principles of adsorption and adsorption process, John Wiley and Sons, London, 1984.

[19] C.N. Satterfield, T.K. Sherwood, The role of diffusion in catalysis, Addison Wesley Pub. Co, Reading (MA), 1963.

[20] H. Lee, G. Thodos, Generalized treatment of self-diffusivity for the gaseous and liquid states of fluids, Ind. Eng. Chem. Fundam. 22 (1983) 17–26.

[21] A.R. Mitchell, Computational Methods in Partial Differential Equation, John Wiley and Sons, London, 1969.

[22] J.H. Ferziger, Numerical Methods for Engineering Application, John Wiley and Sons, London, 1981.

[23] B.P. Leonard, A stable and accurate convective modelling procedure based on quadratic upstream interpolation, Comput. Meth. Appl. Mech. Eng. 19 (1979) 59–98.

[24] W.H. Press, S.A. Teukolsky, W.T. Vetterling, B.P. Flannery, Numerical Recipes in Fortran, the Art of Scientific Computing, second ed., Cambridge University Press, Cambridge, 1992.

[25] S.C. Chang, J.A. Roux, Thermodynamic analysis of a solar zeolite refrigeration system, J. Sol. Energy Eng. 107 (1985) 189–195.

[26] G. Cacciola, G. Cammarata, L. Marletta, G. Restuccia, Macchine ad adsorbimento a ciclo rigenerativo, La Termotecnica 47 (4) (1993) 81–90.

[27] G. Cacciola, A. Hajji, G. Maggio, G. Restuccia, Dynamic simulation of a recuperative adsorption heat pump, Energy 18 (1993) 1125–1137.

[28] N. Douss, F.E. Meunier, L.-M. Sun, Predictive model and experimental results for a two-adsorber solid adsorption heat pump, Ind. Eng. Chem. Res. 27 (1988) 310–316.

[29] F. Poyelle, J.J. Guilleminot, F. Meunier, I. Soidé, Experimental tests of a gas-fired adsorptive air conditioning system, in: Proceedings of the International Absorption Heat Pump Conference, Montréal, Canada, vol. 1, 1996, pp. 221–229.

[30] D.W. Breck, Zeolite Molecular Sieves, John Wiley and Sons, New York, 1964.

[31] J.J. Guilleminot, A. Choisier, J.B. Chaflen, S. Nicolas, J.L. Reymoney, Heat transfer intensification in fixed bed adsorbers, Heat Recovery Syst. CHP 13 (1993) 297–300.